A secular variation candidate model for IGRF-13 based on Swarm data and ensemble-based inverse geodynamo modelling

A. Fournier, J. Aubert, V. Lesur, G. Ropp
Institut de Physique du Globe de Paris
October 1, 2019

This document presents the methodological backbone used by our group to design a secular variation candidate model for years 2020–2025. A geomagnetic field model centered around 2019.0 is first constructed, based on Swarm data, for both the main field and its instantaneous secular variation (hereafter SV). This initial model and its uncertainties are next fed into an inverse geodynamo modelling framework in order to specify, for epoch 2019.0, an ensemble of 100 initial conditions for the integration of a three-dimensional numerical dynamo model. We use the results of this ensemble of deterministic integrations between years 2020.0 and 2025.0 to propose a time-average secular variation model for that time frame (this SV model is thus centered on 2022.5), along with uncertainties deduced from the statistical properties of the ensemble.

1 Construction of the initial model

1.1 Data selection

We consider vector data for satellite A from epoch 2018.5 to epoch 2019.5 (We dot not utilize magnetic intensity data.) We use systematically the latest version of the data and select first the reprocessed data (SW_OPER_MAGA_LR), then, depending on the epoch, either version 0505 (for the most part) or version 0506.

Data selection differs depending on the geomagnetic latitude. We distinguish high-latitude (HL henceforth) data from mid-latitude (ML henceforth) data. HL (resp. ML) data correspond to a geomagnetic latitude of absolute value larger (resp. smaller) than 55°.

The following selection criteria apply:

- ML data are selected for local times between 11:00 pm and 5:00 am, and rejected for sunlit ionosphere.
- Data are selected for positive values of the vertical component of the interplanetary magnetic field (IMF): $B^Z_{IMF} > 0$.
- Data are selected for D_{st} values inside $[-30 : 30]$ nT and its time variation $\dot{D}_{st}$ between $[-100 : 100]$ nT/day: we are interested in the low-frequency component of the signal measured during quiet times.
- ML data are sampled every 30 seconds, while HL data are sampled every 60 seconds. This corresponds to collecting one point approximately every degree along the satellite track.

The size of the corresponding data vector is $493,836$ ($=3\times164,612$). Note that HL data are handled in the usual North, East, Center (NEC) reference frame, whereas ML data are used in a Solar Magnetic (SM) reference frame, reducing this way the correlations between vector data component errors.

Comp.	ML	HL
X	9 nT^2	100 nT^2
Y	9 nT^2	144 nT^2
Z	36 nT^2	100 nT^2

Table 1: Variances prescribed to the three components of mid-latitude (ML) and high-latitude (HL) vector data.

1.2 Data weights

The variances attributed to each type of data are given in Table 1. The inverse of the variance is used to weigh the data when constructing the initial model.

1.3 Modelling method and initial model parameterization

The approach used to build this model is to fit data through a robust re-weighted iterative least-squares process, using Huber weights. The first iteration is a standard L2-norm least-squares inversion.

The magnetic field potential V is represented using a spherical harmonic expansion of the form

$$\begin{aligned} V(r,\theta,\varphi,t) &= V_i(r,\theta,\varphi,t) + V_e(r,\theta,\varphi,t) \\ &= a\sum_{\ell=1}^{L_i}\left(\frac{a}{r}\right)^{\ell+1}\sum_{m=0}^{\ell}\left[g_\ell^m(t)\cos(m\varphi) + h_\ell^m(t)\sin(m\varphi)\right]\mathcal{P}_\ell^m(\cos\theta) \\ &+ a\sum_{\ell=1}^{L_e}\left(\frac{r}{a}\right)^{\ell}\sum_{m=0}^{\ell}\left[q_\ell^m(t)\cos(m\varphi) + s_\ell^m(t)\sin(m\varphi)\right]\mathcal{P}_\ell^m(\cos\theta)\,, \end{aligned}$$

in which (r,θ,φ) denote the standard spherical coordinates, t is time, a is the mean radius of the Earth ($a = 6371.2$ km), L_i is the truncation of the spherical harmonic expansion of the internal sources, and L_e the truncation of the expansion of the external sources. The $\mathcal{P}_\ell^m$ are the associated Legendre functions of degree ℓ and order m, whose normalization is subject to the Schmidt convention.

The description of internal and external sources is done according to the guidelines provided by Holschneider et al. [2016]. The idea is essentially to over-parameterize the contribution of each source and to constrain the resulting parameters using physical prior information.

Prior information on the model components is provided through the description of a Gaussian model distribution characterised by a mean and a covariance matrix. For all model sources the mean is zero. Except for the main field and its SV, the model covariance matrix for a given component is defined as in Holschneider et al. [2016], in terms of a radius and a scaling factor.

1.3.1 Internal sources

The truncation applied for internal sources is $L_i = 30$. The main (dynamo) field is described up to spherical harmonic degree 18, and so is its secular variation. The secular variation is assumed to be constant between 2018.5 and 2019.5, and consequently the Gauss coefficients to vary linearly with

time over this time frame. The prior information used to constrain these Gauss coefficients is based on the multivariate statistics of a 70,000 year long free run integration of the coupled Earth dynamo model by Aubert et al. [2013]. This choice is motivated by the will to ensure consistency between the initial model and the forecast that is produced using the same numerical model (more on the forecast below).

The crustal field is expanded in spherical harmonic degree from degree 15 to degree $L_i = 30$ (prior covariance properties: radius 6280.0 km, scaling factor= 2.7 10^{-2}). A known crustal field [Lesur et al., 2013] is subtracted from the data for degrees 30 to 110.

The induced mantle field is described up to spherical harmonic degree 3, and each of its spherical harmonic component is assumed to be proportional to the internal component of the D_{st} index (prior covariance properties: radius=2 537 km, scaling factor=1.0).

1.3.2 External sources

The external sources considered are the following:

- A static external field in the Geocentric Solar Magnetopsheric (GSM) coordinate system for the remote magnetosphere (prior covariance properties: radius=16 000 km, scaling factor=5400)
- A static external field in the Solar magnetic (SM) coordinate system for the near magnetosphere (prior covariance properties: radius=6 900 km, scaling factor=3.56)
- A time-varying external field dependent upon the external D_{st} index (prior covariance properties: radius=16 000 km, scaling factor=5.4)
- A time-varying external field dependent on the Y component of the IMF in the SM coordinate system (prior covariance properties: radius=6 900 km, scaling factor=0.1)

Each of these external sources is described up to spherical harmonic degree $L_e = 3$.

1.3.3 The initial model

The initial model, centered on 2019.0, is obtained after 3 iterations. Of particular interest for the prediction of the SV to be described below are the sets of Gauss coefficients of the main field and its SV at epoch 2019.0, along with their associated posterior covariance matrices $\mathbf{C}_{MF}$ and $\mathbf{C}_{SV}$, respectively. The fit to the data (weighted by the the Huber weight to data ratio) is 1.31 nT.

2 Ensemble-based inverse geodynamo modelling

2.1 Principle

Our approach is similar to the one followed for our contribution to IGRF-12 [Fournier et al., 2015]. With the initial model (and its error covariance matrices $\mathbf{C}_{MF}$ and $\mathbf{C}_{SV}$) at hand, we next apply the inverse geodynamo modelling framework of Aubert [2014] with a few novel features, namely an

ensemble approach to deal with uncertainties and the possibility to enforce a QG-MAC force balance for the initial condition to be prescribed [Aubert, in prep.]. The numerical dynamo model we resort to is the coupled Earth dynamo [Aubert et al., 2013].

The multistep approach can be summarized as follows:

1. 100 decorrelated independent dynamo states are extracted from a 70,000 year long free run integration of the coupled Earth Dynamo.
2. For each ensemble member e, a Kalman filter estimates the three-dimensional structure of the magnetic field $\mathbf{B}_e$(dyn,3D) in the core interior from the field provided by the initial model $\mathbf{B}$(obs) and the prior information based on the statistics (mean and covariance) of the 70,000 year long free run integration.
3. For each ensemble member, the knowledge of the three-dimensional magnetic structure inside the core makes it possible to compute the three-dimensional magnetic diffusion inside the core, $\mathbf{D}_{\mathrm{mag},e}$.
4. We next solve a diffusion-free core-flow problem at the core surface, seeking the core surface field $\mathbf{u}_{s,e}$ which satisfies
$$\hat{\boldsymbol{r}} \cdot \left[\dot{\mathbf{B}}(\text{obs}) - \mathbf{D}_{\mathrm{mag},e} \right] = -\boldsymbol{\nabla}_h \cdot \left(\mathbf{u}_{s,e}\, \hat{\boldsymbol{r}} \cdot \mathbf{B}_e(\text{dyn,3D}) \right),$$
where $\hat{\boldsymbol{r}}$ is the unit vector in the spherical radial direction. This problem is solved under the weak constraint that the QG-MAC balance is satisfied at the core surface [Aubert, in prep.].
5. Finally, another Kalman filter converts this estimate of $\mathbf{u}_{s,e}$ into a three-dimensional estimate of the flow and buoyancy fields, for this member of the ensemble.

The three-dimensional estimates of the buoyancy, magnetic field and flow define a unique initial condition for the integration of the numerical dynamo model, details of which can be found in the study of [Aubert et al., 2013, and references therein]. This integration is performed for each ensemble member e.

2.2 Dynamic vs steady flows

Validation tests carried out between 2015.0 and 2019.3 showed us that our strategy is superior to a linear extrapolation of the field. The same validation tests further demonstrated that a steady flow assumption provides a more conservative and consistently better estimate than that obtained with the dynamic calculation. The steady flow assumption is thus the one retained for the candidate model. The relevant quantitative measures of success of the various tests we conducted will be provided in the paper that will document our candidate model.

3 Secular variation candidate

3.1 Definition

For each ensemble member e, we compute
$$\frac{\mathbf{B}_e(2025.0) - \mathbf{B}_e(2020.0)}{5 \text{ years}}$$

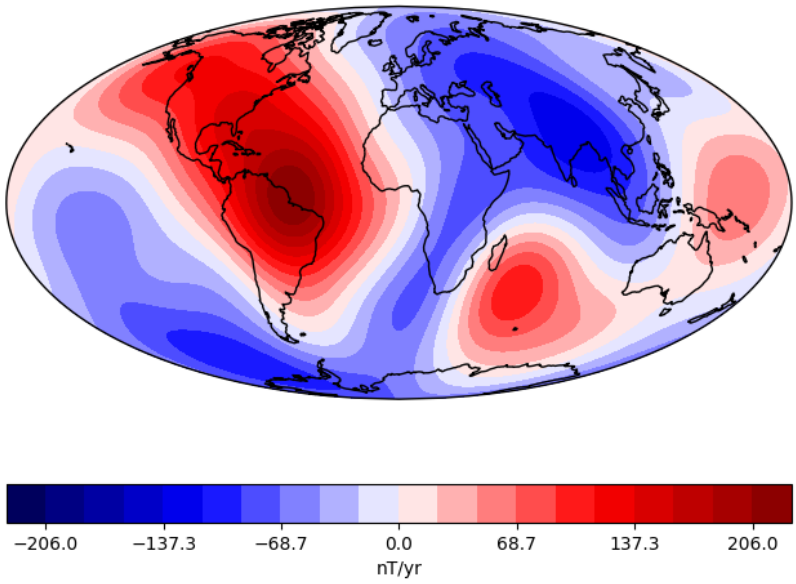

Figure 1: Radial component of the average secular variation (truncated at spherical harmonic degree 8) at Earth's surface for the 2020-2025 period.

at the surface of the Earth (mean spherical radius 6371.2 km). Our candidate model is the median of this ensemble of average SV predictions. This candidate is shown in Figure 1.

3.2 Uncertainties

The uncertainties are given by the 90% credible interval for each Gauss coefficient of the ensemble of 100 predicted SV.

References

Julien Aubert. Earth's core internal dynamics 1840–2010 imaged by inverse geodynamo modelling. *Geophysical Journal International*, 197(3):1321–1334, 2014.

Julien Aubert. Recent geomagnetic variations and the force balance in earth's core, in prep. To be submitted.

Julien Aubert, Chrisopher C. Finlay, and Alexandre Fournier. Bottom-up control of geomagnetic secular variation by the Earth's inner core. *Nature*, 502:219–223, 2013. doi: 10.1038/nature12574.

Alexandre Fournier, Julien Aubert, and Erwan Thébault. A candidate secular variation model for IGRF-12 based on swarm data and inverse geodynamo modelling. *Earth, Planets and Space*, 67 (1):1–17, 2015.

Matthias Holschneider, Vincent Lesur, Stefan Mauerberger, and Julien Baerenzung. Correlation-based modeling and separation of geomagnetic field components. *Journal of Geophysical Research: Solid Earth*, 121(5):3142–3160, 2016. doi: 10.1002/2015JB012629.

V. Lesur, M. Rother, F. Vervelidou, M. Hamoudi, and E. Thébault. Post-processing scheme for modeling the lithospheric magnetic field. *Solid Earth*, 4:105–118, 2013. doi: 10.5194/sed-4-105-2013. URL www.solid-earth.net/4/105/2013/.

Acknowledgements

We acknowledge support from CNES and the Fondation Del Duca of Institut de France (JA, 2017 Research Grant). Numerical computations were performed at S-CAPAD, IPGP. ESA is acknowledged for the provision of the Swarm data and for the principal investigator status granted following the Swarm Science and Validation call and selection. AF thanks Clemens Kloss for the chaosmagpy python library used during the testing phase of our workflow.